AIP Advances

Inverted-parabolic and weak strain dependencies on the critical current in practical <110> and <100> oriented REBCO tapes

Cite as: AIP Advances **9**, 075216 (2019); https://doi.org/10.1063/1.5092248
Submitted: 08 February 2019 . Accepted: 10 July 2019 . Published Online: 22 July 2019

Kozo Osamura, Shutaro Machiya, Kentarou Kajiwara, Takuro Kawasaki, Stefanus Harjo, Yifei Zhang, Shinji Fujita, Yasuhiro Iijima, and Damian P. Hampshire

Inverted-parabolic and weak strain dependencies on the critical current in practical <110> and <100> oriented REBCO tapes

Cite as: AIP Advances 9, 075216 (2019); doi: 10.1063/1.5092248
Submitted: 8 February 2019 • Accepted: 10 July 2019 •
Published Online: 22 July 2019

Kozo Osamura,[1,a)] Shutaro Machiya,[2] Kentarou Kajiwara,[3] Takuro Kawasaki,[4] Stefanus Harjo,[4] Yifei Zhang,[5] Shinji Fujita,[6] Yasuhiro Iijima,[6] and Damian P. Hampshire[7]

AFFILIATIONS

[1]Research Institute of Applied Sciences, Kyoto 606-8202, Japan
[2]Department of Engineering, Daido University, Nagoya 457-8530, Japan
[3]JASRI, 1-1-1 Kouto, Sayo-cho, Hyougo 679-5198, Japan
[4]J-PARC Center, 2-4 Shirane Shirakata, Tokai-mura, Ibaraki 319-1195, Japan
[5]SuperPower Inc., 450 Duane Ave., Schenectady, New York 12304, USA
[6]Advanced Technology Laboratory, Fujikura Ltd., 1440, Mutsuzaki, Sakura-shi, Chiba 285-8550, Japan
[7]Department of Physics, University of Durham, Durham DH1 3LE, UK

[a)]**Corresponding author:** Kozo Osamura (kozo_osamura@rias.or.jp)

ABSTRACT

In the commercial coated conductor tapes, the twinned structure of REBCO ($REBa_2Cu_3O_{7-d}$, RE = Y and Gd) is characterized as either <100> or <110> orientation based on the tape length direction. In this study, we investigate the effects of the two different twinned structures on the critical current I_c of the REBCO tapes by combining; transport critical current and synchrotron radiation diffraction measurements. For the tapes with <100> oriented twins, we observed the inverted parabolic strain behavior on the uniaxial strain dependence of I_c. In contrast, the ones with <110> oriented twins showed a weak strain behavior without any maximum appeared in the strain dependence. Such a different uniaxial strain dependence was analyzed by using the one-dimensional twin model with different fractional lengths of A-domains and B-domains of REBCO twins. This model explains the essential features of the different uniaxial strain dependence we observed.

I. INTRODUCTION

Despite the extensive efforts develop practical composite superconductors, there are only five materials that have been commercialized.[1] These practical superconducting wires and tapes have the multi-component composite structures designed to meet various kinds of the sophisticated engineering requirements. Because the constituent components have different coefficients of thermal expansion (CTE) and different moduli of elasticity (E), it is difficult to determine the local stress and strain exerted on the superconductor components and how they influences the electromagnetic properties under the actual operating conditions.[2] Several analyses of the local stress and strain have been reported for the commercialized superconductors such as MgB_2,[3] BSCCO,[4,5] REBCO[6–8] and Nb_3Sn,[9–12] all of which are the brittle material. The nature and origin of the stress and strain behavior on the electromagnetic properties depends on the conductor architecture as well as these material systems. The quantitative studies of these material systems embedded in the actual conductors are of significant importance to unleash the conductor potential under the stress and strain conditions that the superconductor devices are actually operated.

TABLE I. Characteristic dimension of the components of REBCO tapes investigated in the present project.

Sample Name	REBCO <100> without Cu	REBCO <100> with Cu	REBCO <110> with Cu
Tape thickness (mm)	0.054	0.070	0.22
Tape width (mm)	4.0	2.0	5.0
Thickness of Hastelloy substrate (micron)	50	50	100
Thickness of Cu lamination (micron)	no	15	100
REBCO thickness (micron)	1.65	1.65	1.1
Rare earth element of REBCO layer	$Y_{0.5}Gd_{0.5}$	$Y_{0.5}Gd_{0.5}$	Gd

It has been well-established that the I_c - strain dependence of practical Nb_3Sn wires shows the I_c maximum[13–15] at the strain values close to the zero deviatoric strain.[16] In case of the practical BSCCO-2223 tapes, it is less clear whether such an I_c maximum exists in the reversible region. But it appears that the observed I_c maximum in the strain dependence correlates to the degradation caused by the compressive fracture of BSCCO-2223 filaments.[17] The elastic regime for BSCCO-2223 tapes has a weak strain behavior that is qualitatively quite different to the inverted parabolic behavior of Nb_3Sn.

Since various projects utilizing the REBCO tapes started, their mechanical and electromagnetic properties have been investigated widely.[18,19] The commercial REBCO ($REBa_2Cu_3O_{7-d}$, RE = Y and Gd) tapes were found to have either <100> or <110> direction of their REBCO layer aligned along their tape axis. Recently we found that the <100> oriented REBCO tapes exhibit an inverted parabolic strain dependence with a clear maximum of the critical current, that presumably is associated with the supercurrent passing between the A- and B- domains of REBCO twins.[20] The focus of this study is to determine the strain dependence of I_c of the <110> oriented REBCO tape. In particular we investigated whether the <110> oriented REBCO tapes show the I_c maximum in the strain dependence of I_c. We also compared the results of the <100> and <110> oriented REBCO tapes and showed that the different strain dependencies can be explained by the one-dimensional twin (or chain) model.[20]

The strain dependence of I_c over a wide range of external uniaxial strain was investigated by the free-standing sample holder and the springboard.[21] Furthermore, in order to directly access the local strain exerted on the REBCO superconductor layer, the synchrotron diffraction measurement was performed at SPring-8.[20]

II. EXPERIMENTAL PROCEDURE

We studied the two REBCO tapes from SuperPower and the one from Fujikura. Both of SuperPower tapes have the <100> direction of REBCO aligned along the tape axis, whereas the Fujikura tape has the <110> direction along the tape axis. The primary difference between two SuperPower tapes is whether it has the outmost Cu layer. The general specifications of these tapes are tabulated in Table I as can also be found at the manufacturer's web-pages.[22,23] From now on, we call the SuperPower tapes with and without Cu as "REBCO <100> with Cu" and "REBCO <100> without Cu", respectively, and the Fujikura tape as "REBCO <110> with Cu". In general, these coated conductor tapes consist of a thin superconducting layer grown on top of the buffer layers that are formed on the metal substrate.

The critical current (I_c) measurements were carried out in the open cryostats filled with liquid nitrogen. The experimental details of the free-standing transport measurements using the springboard reported elsewhere.[20] The freestanding samples were held using the gripping jig which was electrically isolated from the universal testing machine (Fig. 1 (a)). The voltage taps were soldered

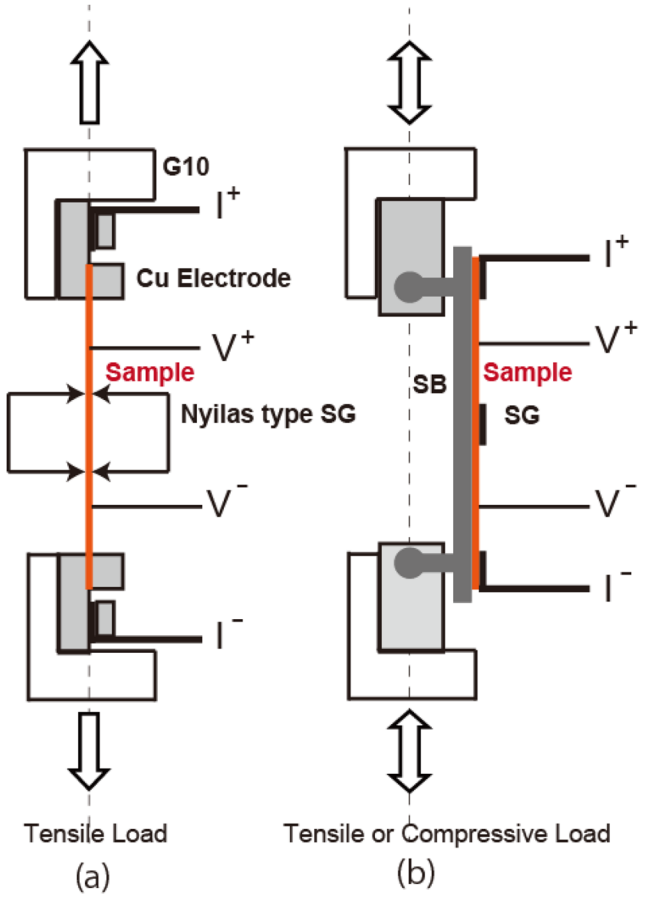

FIG. 1. Two techniques (a) and (b) for evaluating the uniaxial strain dependence of I_c, where G10 is an insulator, SG is a strain gauge, and SB is the springboard.

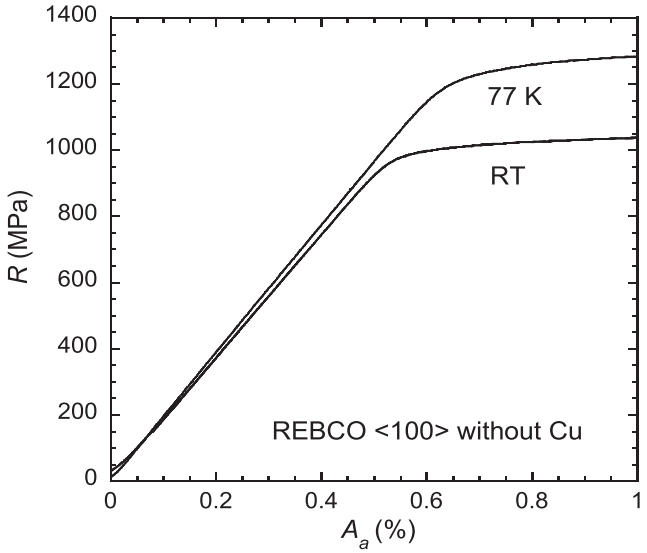

FIG. 2. Stress – strain curve at RT and 77 K for REBCO <100> without Cu.

25 mm apart onto the tape, outside the Nyilas type extensometer. The critical current was determined with using a criterion of 1 μV/cm. For the measurements using the springboard (Fig. 1 (b)), the tape sample was soldered onto the springboard, and then the strain gauge was glued onto the tape surface. The springboard enables us to apply both compressive and tensile strains to the tapes by pushing or pulling along the load axis. The changes in strain produced by the springboard were then measured by the strain gauge.

The diffraction experiments were carried out at room temperature at the BL28B2 station in SPring-8.[20] As we did for the Ic measurements stated earlier, the freestanding samples and the ones attached with the springboard were both measured. For the freestanding samples, the Nyilas type extensometer was placed outside of the area exposed to the X-ray incident beam so as to prevent it from the beam exposure. The samples attached to the springboard were placed in a specially designed load frame. The size of the Cu-Be springboard was 78 mm long, 15 mm wide and 2.5 mm thick. In order to reduce the absorption of incident X-ray, the blind hole was incorporated into the spring board. We evaluate that the present small blind hole does not damage decisively any uniform deformation of the spring board for the present purpose of study. The shift and/or broadening of diffraction peaks as a function of uniaxial strain were measured for these samples. The diffraction geometry confirmed that the scattering vector was parallel to the tape axis. In this study, the lattice spacing of (200), (020) and (220) planes of the orthorhombic REBCO was characterized so as to evaluate the local strain. The diffraction intensity of these peaks was strong enough to provide sufficient accuracy in statistics. In a further detailed investigation, we need to consider the effect of the lattice constant of the buffer layer when comparing the property of two types of commercial <110> and <100> oriented BEBCO tapes.

III. EXPERIMENTAL RESULTS

A. Mechanical properties at room temperature (RT) and 77 K

Fig. 2 shows the stress (R) – strain (A_a) behavior at RT and 77 K for the REBCO <100> without Cu. The slope is linear in the small strain region. At the high strain regions, the tapes as a whole did not fracture even beyond the shoulder in the response. But we observed the plastic deformation associated with work hardening of the metal components in the tape. The modulus of elasticity was determined in the linear – small strain region according to the method recommended by the international standard IEC 61788-25.[24] Here we considered the two types of the modulus of elasticity, E_0 and E_u, that are defined by the initial slope of the stress – strain curve and the slope of the partially unloaded curve, respectively. Usually the international standard recommends that E_u is recorded as the standard values as well as the stress and strain at the 0.2% proof strength $R_{0.2}$ and $A_{0.2}$. Table II shows the mechanical properties for all tested tapes including the REBCO <100> with and without Cu and the REBCO <110> with Cu. As expected, the modulus of elasticity of the with a Cu is lower than the one without Cu.

B. Tensile load dependence of critical current—Free standing measurements

Previous studies[19,20] made clear that the I_c of REBCO tapes decreases over a small range of tensile stress and then the I_c returns reversibly when the stress reduces back to zero. When the tensile stress is increased beyond the characteristic limit, the I_c drops sharply due to the fracture of brittle REBCO layer. This behavior was reconfirmed for our tested REBCO tapes as shown in Fig. 3 and 4. Fig. 3 represents the normalized I_c (I_c/I_{c0} and I_{cr}/I_{c0}) for REBCO <100> without Cu as a function of the applied strain (A_a).

TABLE II. Summary of mechanical properties for three REBCO tapes.

Sample Name	Temperature	E_U (GPa)	$R_{0.2}$ (MPa)	$A_{0.2}$ (%)
REBCO <100> without Cu	RT	185	1021	0.748
	77K	194	1270	0.855
REBCO <100> with Cu	RT	166	876	0.738
	77K	168	1076	0.857
REBCO <110> with Cu	RT	141	744	0.716
	77K	168	960.5	0.755

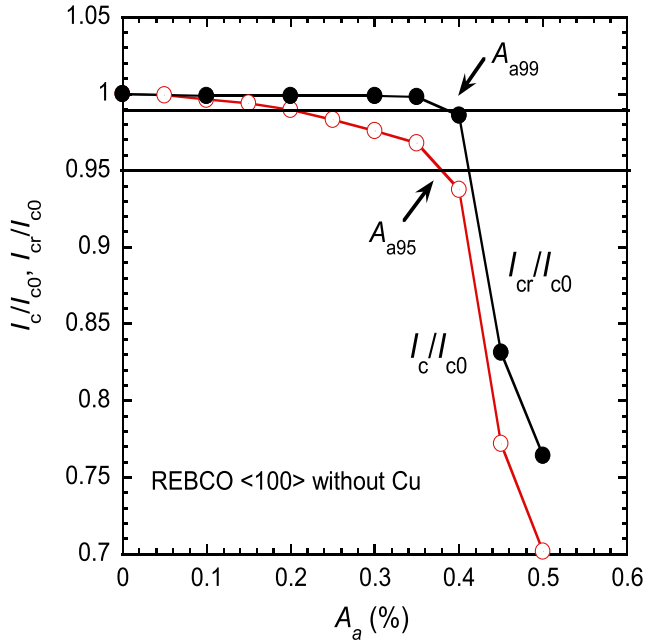

FIG. 3. Applied strain dependence of normalized critical currents, I_c/I_{c0} and I_{cr}/I_{c0} for REBCO <100> without Cu.

The I_c/I_{c0} decreases gradually from the beginning and then stars decreasing more rapidly over the strain region larger than 0.38%. Also, the normalized recovered I_{cr} (denoted as I_{cr}/I_{c0} in Fig. 3) decreases very slowly up to about 0.4% of strain and then starts dropping suddenly beyond that point. The radical decrease of J_c/J_{c0} and J_{cr}/J_{c0} is attributed to the fracture of brittle REBCO layer.[19]

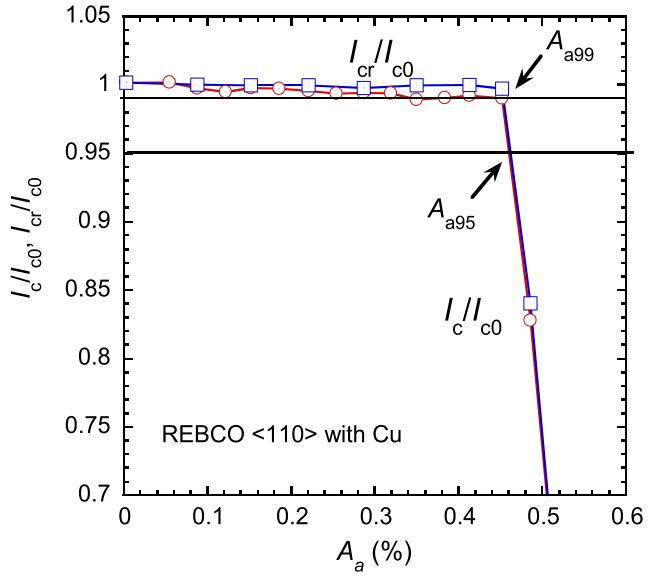

FIG. 4. Applied strain dependence of normalized critical currents, I_c/I_{c0} and I_{cr}/I_{c0} for REBCO <110> with Cu.

As shown in Fig. 3, the recovered critical current I_{cr} decreases rapidly beyond a certain strain. We discussed in our previous studies that the reversible stress limit is best defined as the stress at I_{cr}/I_{c0}=0.99[20] for which the reversible stress and strain limits is expressed as R_{99} and A_{a99}, respectively. As listed in Table III, R_{99} was 760 MPa for REBCO <100> without Cu. The similar stress - strain dependence on the I_c/I_{c0} and I_{cr}/I_{c0} was measured for REBCO <100> with Cu and the corresponding critical parameters are also summarized in Table III.

Fig. 4 shows the I_c/I_{c0} and I_{cr}/I_{c0} as a function of applied strain for REBCO <110> with Cu. Compared with REBCO <100> without Cu of Fig. 3, both I_c/I_{c0} and I_{cr}/I_{c0} are far less sensitive to the strain or stress in the reversible region. As seen in Table III, A_{99} before rapid decrease of I_{cr}/I_{c0} was 0.455%. The other groups also used the 95% retained strain (A_{a95}) convention to the reversible strain limit for both REBCO and BSCCO tapes.[8,17,21] Thus, A_{a95} and R_{95} were also evaluated and shown in Table III.

C. Uniaxial strain dependence of critical current—Springboard measurements

The similar I_c measurements were carried out for all of those tapes mounted on the springboard. As shown in the upper of Fig. 5, the I_{cr}/I_{c0} of REBCO <100> without Cu kept almost constant over the measured strain region (i.e. -0.4% to 0.6%), suggesting that there was no observable degradation in the REBCO layer. Its I_c/I_{c0} showed the clear maximum. But this I_c/I_{c0} dependence on strain is not symmetric over the zero strain. Indeed, the peak of the inverted parabola located in the tensile region. In order to discuss the strain dependence, the following parameters were obtained: $A_{a0.98}(-)$=-0.219%, A_{amax}=0.120% and $A_{a0.98}(+)$=0.448%. The I_{cr}/I_{c0} and I_c/I_{c0} dependence on strain of REBCO <100> with Cu is shown in the lower of Fig. 5. In the whole region of measured strain, the values of I_{cr}/I_{c0} were always larger than 0.99, suggesting that no degradation occurred in this sample too. The I_c/I_{c0} maximum appeared approximately at the zero strain. The following parameters of REBCO <100> with Cu were obtained: $A_{a0.98}(-)$=-0.300%, A_{amax}=0.048% and $A_{a0.98}(+)$=0.360%.

Fig. 6 shows the I_c/I_{c0} and I_{cr}/I_{c0} of REBCO <110> with Cu as a function of applied strain. Compared with the two REBCO <100> samples shown in Fig. 5, the strain effect on both I_c/I_{c0} and I_{cr}/I_{c0} is far smaller in the reversible compressive and tensile strain region. We also found A_{a99} = 0.453%, which is the strain just before the I_c starts dropping due to the fracture of brittle REBCO layer.

D. Change of local strain on REBCO layer

Synchrotron diffraction measurements were carried out to directly assess the local strain exerted on the REBCO layer and precisely measure its effect on I_c. As demonstrated in Fig. 7, we paid particular attention to the diffraction peaks from the (200) and (020) crystal planes of REBCO, for which the scattering vector was kept along to the tape axis. Fig. 7 shows the diffraction data of REBCO <100> with and without Cu that was obtained with increasing the tensile strain up to 0.7% with the increment of 0.025%. The peak positions shifted towards the larger lattice spacings as the strain increased.

The change of lattice spacing as a function of applied strain for REBCO <100> with and without Cu is shown in the lower and upper

TABLE III. Summary of 99% recovery and 95% retention.

	99% Recovery		95% Retention	
Sample Name	A_{99} (%)	R_{99} (MPa)	A_{95} (%)	R_{95} (MPa)
REBCO <100> without Cu	0.385	760	0.377	750
REBCO <100> with Cu	0.453	739	0.400	653
REBCO <110> with Cu	0.455	642	0.461	654

of Fig. 8, respectively. The stress-strain curve is also shown in each figure. Their (200) and (020) lattice spacings increased linearly with increasing applied tensile strain up to about 0.5%. Here the solid straight line gives the following relation;

$$d(A) = d(0)[1 + \frac{A_a}{100}] \quad (1)$$

which suggests that the REBCO layer deforms elastically with increasing applied tensile strain. Beyond this linear part, the shoulder appeared in the stress-strain curve that is correlated to the prominent plastic deformation.

The data of Fig. 7 also shows that the intensity profiles of both the (200) and (020) diffraction peaks are rather unchanged. By fitting a Gaussian curve to each diffraction peak, the observed intensity profiles were separated into two profiles and then their ratio (φ) were evaluated as follows,

$$\varphi = \frac{Integrated\ Intensity\ of\ (200) Diffraction}{Integrated\ Intensity\ of\ (020) Diffraction} = \frac{f}{1-f} \quad (2)$$

Fig. 9 represents the ratio (φ) of the integrated intensity of (200) diffraction to that of (020) for both REBCO <100> with and without Cu. The ratio φ remains between 1.11 and 0.96 in the reversible strain region of less than ~0.5%. From the relationship defined by in Eq. (2), the estimated volume fraction f is 0.490 ~ 0.526. The width of the peaks at their half maximum was calculated from the two Gaussian curves and are shown in Fig. 10. The width of the (200) peak

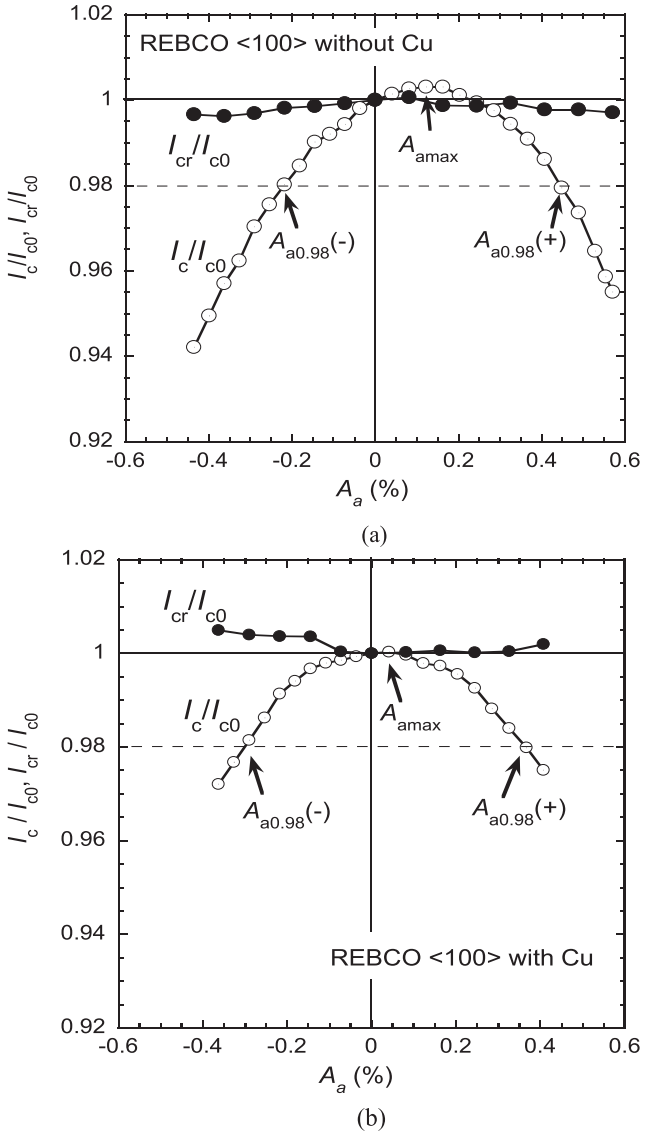

FIG. 5. Uniaxial strain dependence of the normalized critical current for (a) REBCO <100> without Cu and (b) REBCO <100> with Cu.

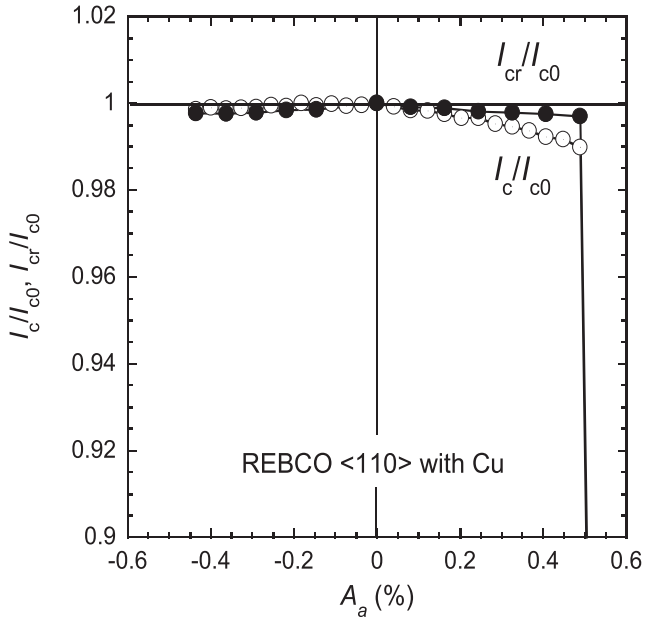

FIG. 6. Uniaxial strain dependence of the normalized critical current for REBCO <110> with Cu.

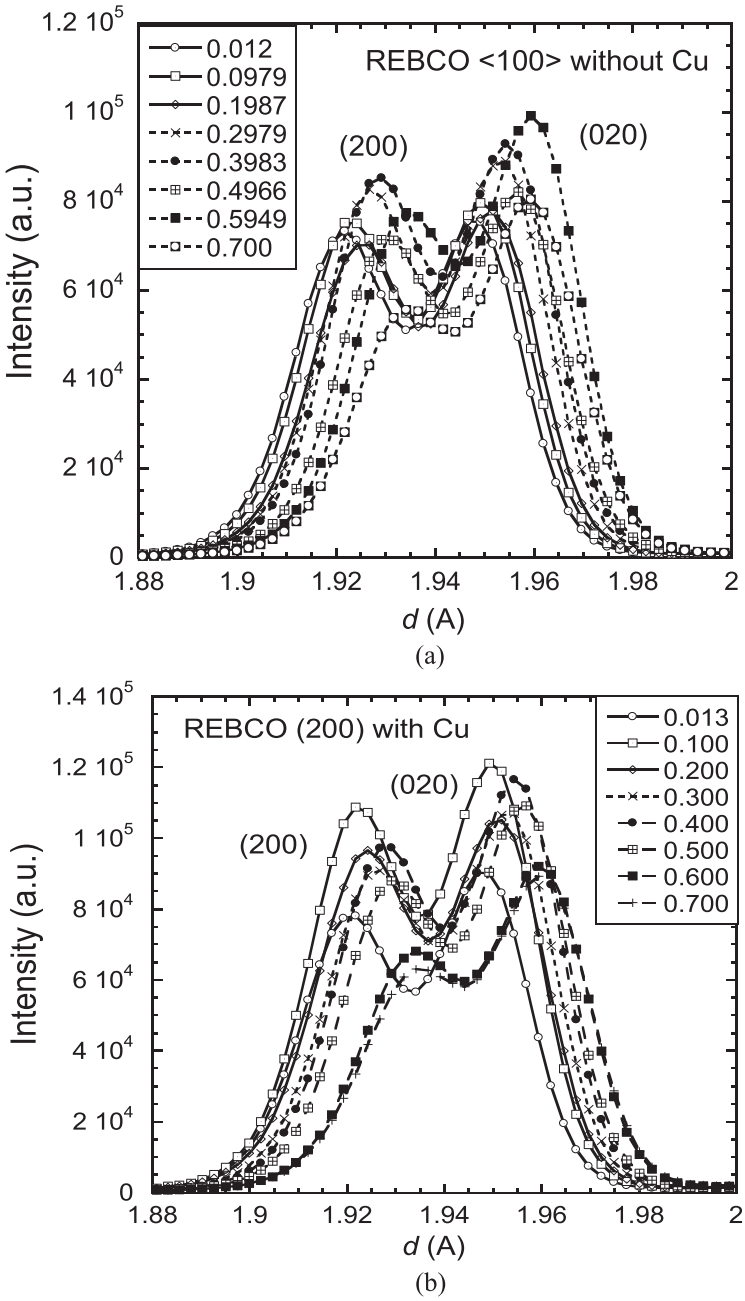

FIG. 7. Typical diffraction profiles of the (200) and (020) planes of the $REBa_2Cu_3O_{8+x}$ phase while increasing the applied tensile strain as indicated in the figure. (a): for REBCO <100> without Cu. (b): for REBCO <100> with Cu.

was broader than that of the (020) in both REBCO <100> with and without Cu.

The profiles of diffraction peaks of REBCO <110> with Cu are shown in Fig. 11. The strain was increased up to 0.5% in steps of about 0.025%. Because the <110> direction of REBCO is parallel to the tape axis, a single diffraction peak from the (220) plane appeared under each tensile strain. As is seen in Fig. 11, the peak position shifts towards the larger lattice spacing. As shown in Fig. 12, the change of lattice spacings as a function of applied strain is plotted along with the stress-strain curve of REBCO <110> with Cu. The lattice spacing increased linearly with increasing the applied tensile strain up to about 0.5%. By using Eq. (1), the solid straight line drawn along the linear part of observed lattice spacings confirmed the elastic tensile deformation without any local fracture.

In order to verify the twinned structure in REBCO <110> with Cu, the diffraction pattern was measured on the same sample that was rotated 45 degrees away from the scattering vector axis.

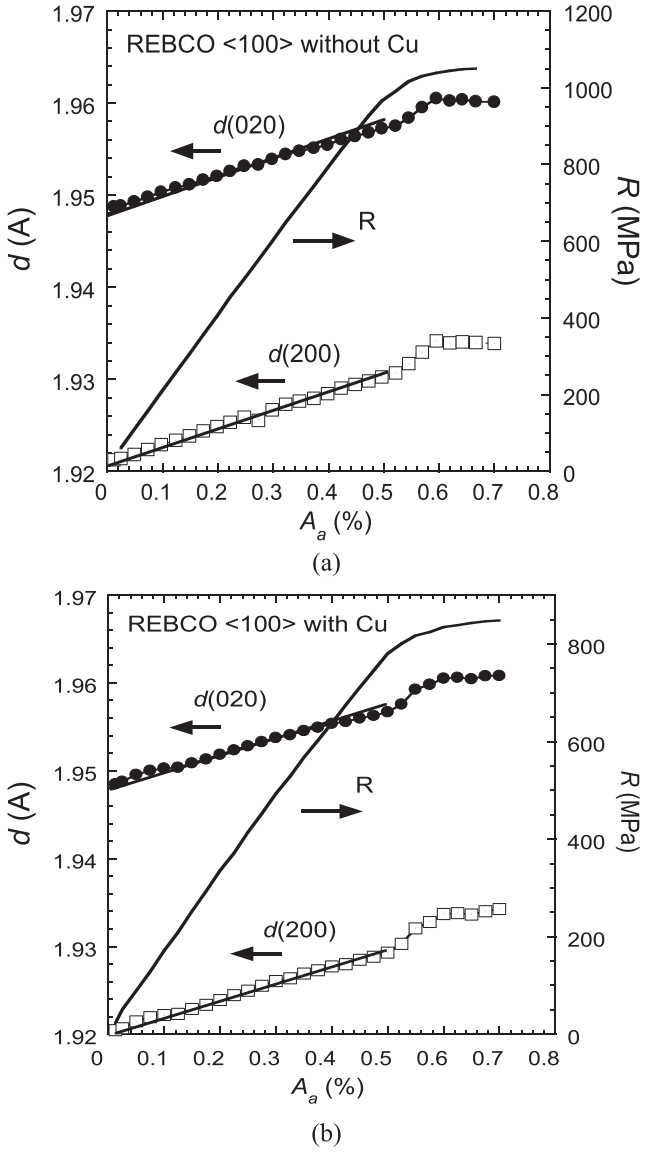

FIG. 8. Applied tensile strain dependence of lattice spacing $d(200)$ and $d(020)$ together with the stress – strain curve. (a): for REBCO <100> without Cu. (b): for REBCO <100> with Cu.

As shown in Fig. 13, the double peak due to (200) and (020) lattice planes was observed. From Eq. (2), the estimated factor f was 0.52.

IV. DISCUSSION AND ANALYSIS

A. One-dimensional twin model for REBCO tapes

The SuperPower tapes (denoted as REBCO <100> with and without Cu) and the Fujukura tape (REBCO <110> with Cu) have the REBCO, whose <100> and <110> aligns parallel to the tape axis, respectively. As shown in Fig. 14 (a), the <100> oriented REBCO has the A[100]- and B[010]- domains alternated one another, forming

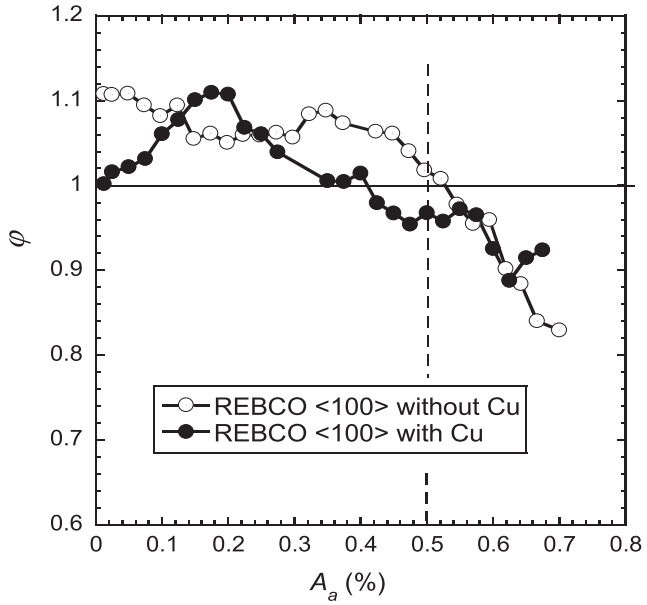

FIG. 9. Tensile strain dependence of the ratio (φ) of the integrated intensity of (200) diffraction to that of (020) one for both REBCO <100> with and without Cu.

the twin boundaries that are 45° tilted with respect to the direction of applying the uniaxial strain. On the other hand, the <110> oriented REBCO has the twin boundaries formed perpendicular to the axis as a result of alternated twins where the a- and b-axis is 45° tilted from the tape axis as shown in Fig. 14 (b). Such a different orientation of twin structure directly affects the strain dependence of I_c.

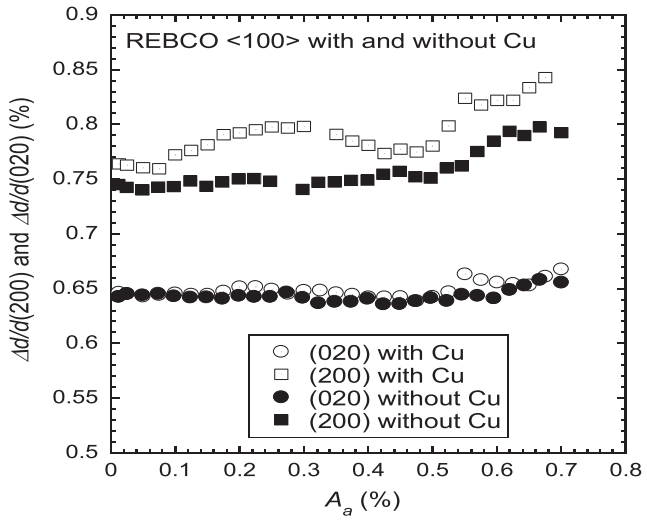

FIG. 10. Width at half maximum intensity divided by the peak (200) and (020) lattice spacings, as a function of applied strain for both REBCO <100> with and without Cu.

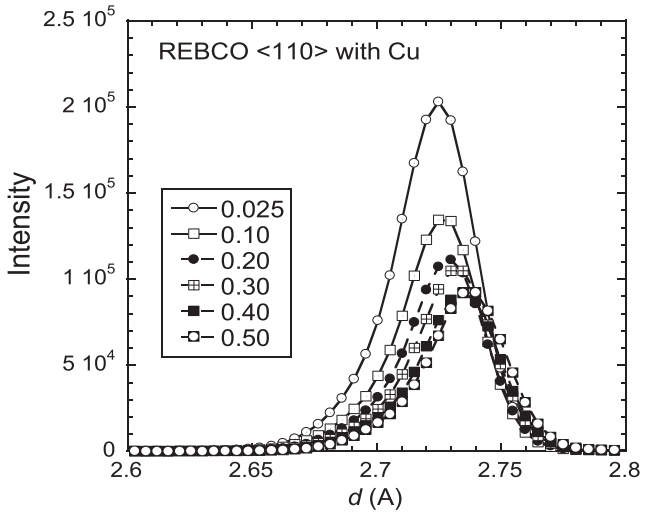

FIG. 11. Diffraction profiles due to (220) plane of $REBa_2Cu_3O_{8+x}$ phase during the increase of applied tensile strain for REBCO <110> with Cu.

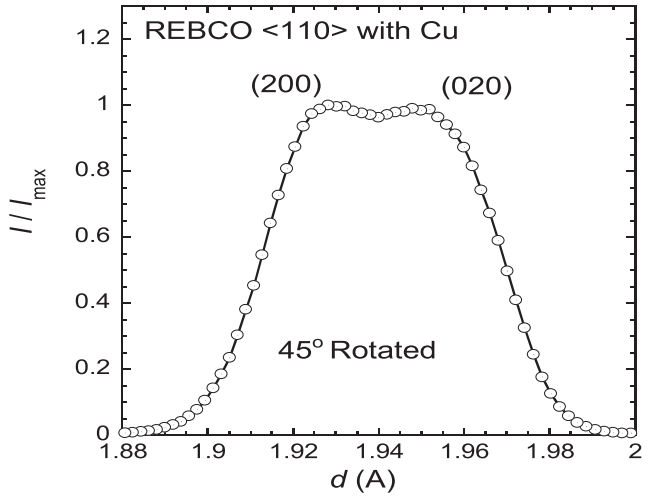

FIG. 13. Diffraction pattern of (200) and (020) lattice planes at the 45 degrees rotated position from the scattering vector axis for REBCO <110> with Cu.

B. Strain dependence of critical current for the <100> oriented tapes

Fig. 14(a) provides an important element of the <100> oriented twin structure, where the current flows across the A[100]- and B[010]- domains over and over. Reference 20 suggested that the strain dependence of I_c is different between the two domains. In each region of Fig. 14(a), the local electric-field – current (E-I) characteristics of a high current superconductor is empirically described by,

$$E = E_C\left(\frac{I}{I_{C,hkl}}\right)^n \tag{3}$$

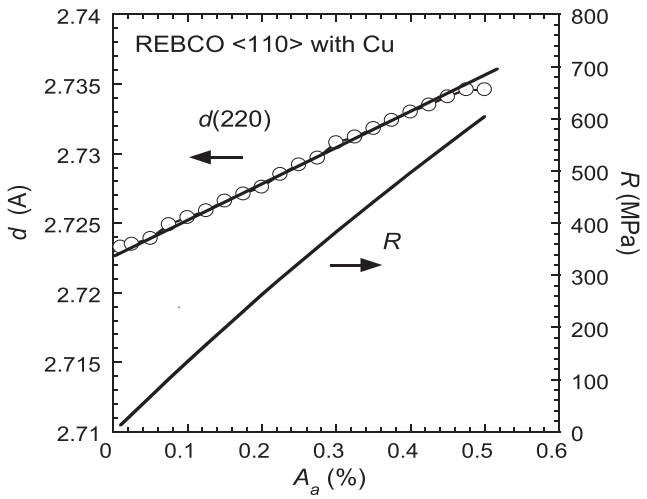

FIG. 12. Applied tensile strain dependence of lattice spacing d(220) together with the stress – strain curve for REBCO <110> with Cu.

where E_C is the electric field at which the critical current I_c is defined and n is known as the index of transition. Following the considerations given in the Annex, the I_c in the A[100]- and the B[010]-domains ($I_{C,100}$ and $I_{c,010}$, respectively) can be described by;

$$I_{C,100} = I_C(0)[1 + g_{100}A_a] \tag{4}$$

$$I_{C,010} = I_C(0)[1 + g_{010}A_a] \tag{5}$$

where A_a is the applied strain, g_{100} and g_{010} are the proportionality constants and $I_c(0)$ is the critical current at zero applied strain. Given the I_c is defined when the electric field E_c becomes 1 μV/cm, the electric field E_c is given by the equation,

$$E_C = fE_{100} + (1-f)E_{010} \tag{6}$$

By using Eqs. (3)–(6), the following relationship is derived,

$$1 = f\left\{\frac{I_C}{I_C(0)(1+g_{100}A_a)}\right\}^n + (1-f)\left\{\frac{I_C}{I_C(0)(1+g_{010}A_a)}\right\}^n \tag{7}$$

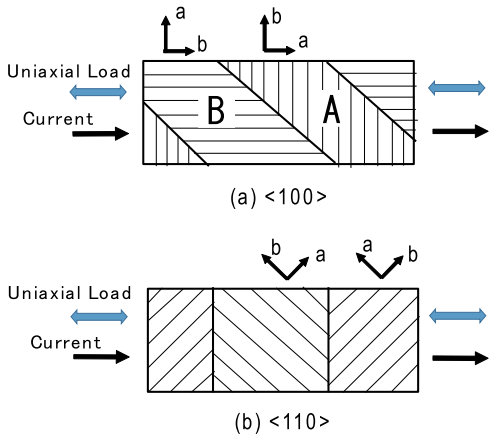

FIG. 14. <100> (a) and <110> (b) oriented twin structures along the tape axis.

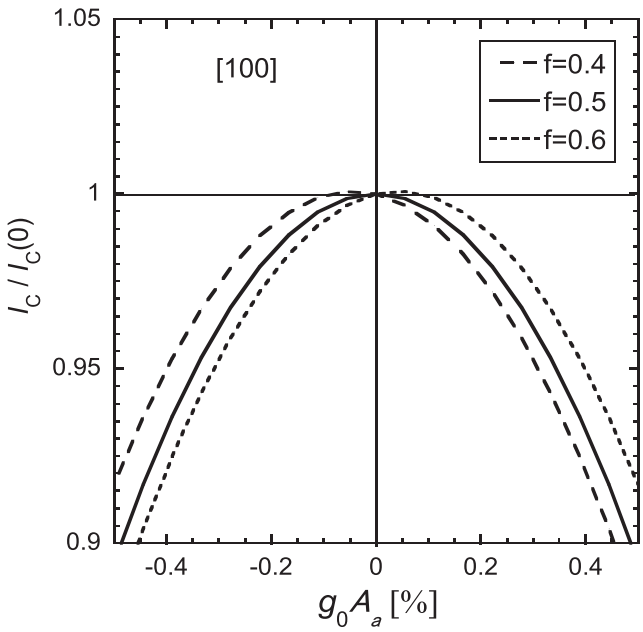

FIG. 15. The normalized critical current as a function of g_0A_a for the <100> oriented tape with different volume ratio of A- and B- domains.

As shown in Fig. 14(a), the A[100]- and B[010]-domains are oriented along the direction of uniaxial strain[25] with the fractional length of two domains given by f and $(1-f)$, respectively. Considering the REBCO a- axis parallel to the loading direction, the Cu-O chains inside the A[100]-domains, are orthogonal to the uniaxial strain. On the other hand, the Cu-O chains in the B[010]-domain are parallel to the uniaxial strain axis and to the current flow direction. So for the <100> tape, we can consider,

$$g_{100} = -g_{010} \equiv g_0 \tag{8}$$

In this case, we take the I_c as reported in Ref. 20 and that is given by,

$$I_C = I_C(0)\{1-(1-2f)g_0A_a - 2(1-f)f(1+n)g_0^2A_a^2 + O[A_a^3]\} \tag{9}$$

Eq. (9) is plotted as a function of applied strain g_0A_a in Fig. 15. We see the very important features here. The one is the inverted parabolic strain behavior for the I_c. The other is the peak position shift. It shifts towards the tensile strain region when the volume fraction f is larger than 0.5, and towards the compressive region with f < 0.5. Also as mentioned previously,[20] the thermal residual strain is induced in the SC layer during cooling, influencing the peak position of I_c as well. The inverted parabolic strain behavior predicted by Eq. (9) is clearly shown in the experimental data of Fig. 5 for the <100> oriented tapes.

C. Strain dependence of critical current for the <110> oriented tape

Fig. 14(b) represents the domain structure of the <110> oriented tape. The a- and b- axis is inclined by 45° tilted against the current flow direction in both A- and B- domains. This means the applied strain affects both of the domains in the same manner. When the external strain is applied along the [100] or [010] direction, the strain changes the lattice constants whose changes are described as $\Delta a/a$ in the a-direction and $\Delta b/b$ in the b-direction, respectively as shown in Fig. 16. Hence the lattice parameter changes along [110] can be approximated by $(\Delta a+\Delta b)/(a^2+b^2)^{1/2}$. In Eq. (8), instead of using the two terms, g_{100} and g_{010}, that are required for the <100> tape, only the single term g_{110} is needed here since both of domains respond to the strain in the same way. Thus, we obtain the following relation,

$$I_C = I_C(0)[1+g_{110}A_a] \tag{10}$$

Unfortunately, there is no detailed study of REBCO single crystals that clearly shows the strain effect on T_C as a function of angle between the a- and b- axis. Hence we assume that the parameter $g(\theta)$ in each domain can be simply approximated as;[26]

$$g(\theta) = g_{100}\cdot\cos(\theta) + g_{010}\cdot\sin(\theta) \tag{11}$$

where θ is the angle between the direction of the applied strain and the a-axis. Eq. (11) is consistent with the limited experimental results of REBCO single crystals showing that a tensile strain along the a-axis direction increases the critical temperature T_C[27] whereas a tensile strain along the b-axis direction decreases T_C. Eq (11) is also consistent with the average angle between the a- and b- axis in a single domain when the tensile components of strain act both a- and b-directions. Indeed, the recent work showed that the <100>

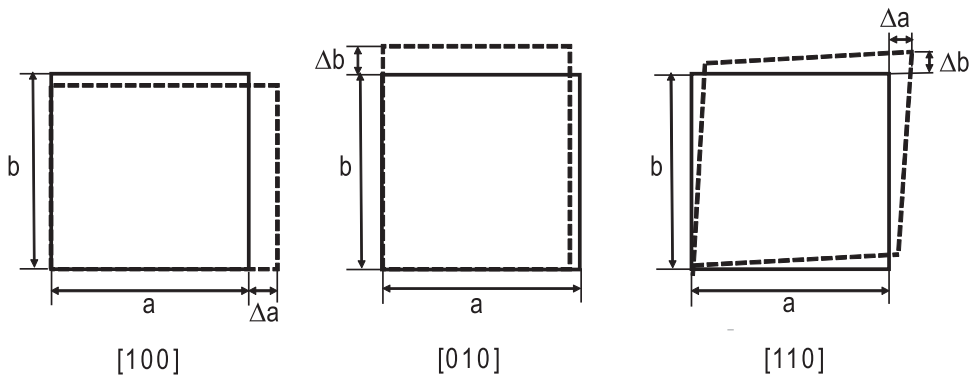

FIG. 16. A principal lattice change by one dimensional deformation along various crystal orientations.

oriented tape exhibits the weak strain behavior with applying the strain along the direction of 45° tilt against the tape axis, whereas the inverted parabolic strain behavior was observed when the strain is applied parallel to the tape direction.[26] For the <110> tapes investigated here, taking into account Eq. (8) with $\theta = 45°$, Eq. (11) leads to:

$$g_{110} = g_{100} \cdot \cos(45^\circ) + g_{010} \cdot \sin(45^\circ) = 0 \quad (12)$$

Hence the resultant external strain dependence of I_c for the <110> tape is given by Eq. (10) for which we expect g_{110} to be small. Indeed, this is zero when Eq. (8) holds. For the <110> tapes, Eq. (10) also has no f– dependence because, as we see in Fig. 14, the relative proportions of the two possible domains do not change the overall strain-dependence of the tape when the direction applied strain is 45° with respect to both the a- and b-axis. We conclude that Eqs. (10) and (12) provide the straightforward explanation for the weak uniaxial strain dependence that we found in the <110> oriented tape shown in Fig. 6.

V. CONCLUSION

In this study, we investigated the two types of commercial tapes of REBCO tapes whose crystal orientation along the tape axis is <100> or <110>. We used the two different I_c measurement techniques to evaluate their uniaxial strain dependence of I_c. On the one technique, we utilized the universal testing machine to which the samples were directly attached and pulled by a tensile load. On the other technique, the samples were soldered on a springboard and then pushed or pulled in order to apply both tensile and compressive strains to the samples. The inverted parabolic behavior was observed on the uniaxial strain dependence of I_c of the <100> oriented REBCO tapes. In contrast, the <110> oriented REBCO tape did not show any I_c maximum on its strain dependence. We used the synchrotron radiation diffraction technique to measure the local strain exerted on the REBCO layer at room temperature by employing the same two techniques stated earlier. Based on the observed data, the local strain exerted on the REBCO layer at 77 K was evaluated and the elastic regime was precisely identified.

The main focus of this study is to explain what causes the different strain dependence of critical current in the <100> and <110> oriented REBCO tapes. The results of these tapes were compared using the common structure model, for which we developed the one-dimensional twin (or chain) model for the REBCO material that presumably possesses the fractional lengths of A-domains and B-domains. Clearly the approach we described in this study can reproduce all broad features of the uniaxial strain dependence of the critical current in those tapes.

ACKNOWLEDGMENTS

This work was supported in part by a grant-in-aid of the Ministry of Education, Culture, Sports, Science and Technology, Japan (26420669). Also it was funded by EPSRC under grant EP/K504178/1. The synchrotron radiation experiments were performed at the BL28B2 of SPring-8 with the approval of the Japan Synchrotron Radiation Research Institute (JASRI) (Proposal No. 2017A1108). The data and materials presented in this paper are on the Durham Research Online website: http://dro.dur.ac.uk/. We acknowledge Dr J Greenwood and Dr F Kametani for their useful discussions and definite proofreading.

APPENDIX

According to the study[27] on the strain-controlled critical temperature in $REBa_2Cu_3O_y$-coated conductors, it was reported that the critical temperature increases with increasing strain along the [100] direction, but it decreases with increasing strain along the [010] one. Their strain dependence can be expressed in the linear form in the small external strain region as follows;

$$T_{C,100} = T_C(0)[1 + q^*_{100}A_a] \quad (A1)$$

$$T_{C,010} = T_C(0)[1 + q^*_{010}A_a] \quad (A2)$$

where A_a [%] is the externally applied strain. By using the original data reported in Ref. 25, the parameters were evaluated as $q^*_{100} = 0.042 \sim 0.046$ and $q^*_{010} = -0.046 \sim -0.042$. So, in order to keep algebra straightforward in our present discussion, we put for the <100> tape that $q_0 = q^*_{100} = -q^*_{010}$. According to the Ekin's scaling law,[16] the magnitude of critical current is related with the critical temperature via the relationship with the upper critical field. Thus, the strain dependence of critical current given by Eqs. (4) and (5) in the main text is assumed to keep the similar dependence with Eqs. (A1) and (A2).

REFERENCES

[1] IEC 61788-20:2014 Superconductivity- Superconducting wires - Categories of practical superconducting wires - General characteristics and guidance.
[2] K. Osamura, S. Machiya, Y. Tsuchiya, and H. Suzuki, "Force free strain exerted on a YBCO layer at 77 K in surround Cu stabilized YBCO coated conductors," Supercond. Sci. Technol. **23**, 045020–045026 (2010).
[3] K. Vinod, R. G. Abhilash Kumar, and U. Syamaprasad, "Prospects for MgB_2 superconductors for magnet application," Supercond. Sci. Technol. **20**, R1–R13 (2007).
[4] K. Osamura, S. Machiya, H. Suzuki, S. Ochiai, H. Adachi, N. Ayai, K. Hayashi, and K. Sato, "Mechanical behavior and strain dependence of the critical current of DI-BSCCO tapes," Supercond. Sci. Technol. **21**, 054010–054018 (2008).
[5] S. Ochiai and H. Okuda, "Residual strain, damage strain and critical current in BSCCO tape," J. Cryo. Soc. Jpn. **46**, 212–219 (2011).
[6] K. Osamura, S. Machiya, Y. Tsuchiya, H. Suzuki, T. Shobu, M. Sato, and S. Ochiai, "Microtwin structure and its influence on the mechanical properties of REBCO coated conductors," IEEE Transactions on Applied Superconductivity **22**, 8400809 (2012).
[7] K. Ilin, K. A. Yagotintsev *et al.*, "Experiments and FE modeling of stress–strain state in ReBCO tape under tensile, torsion and transverse load," Supercond. Sci. Technol. **28**, 055006 (2015).
[8] T. Suzuki, S. Awaji, H. Oguro, and K. Watanabe, "Applied strain effect on superconducting properties for detwinned (Y,Gd)BCO coated conductor," IEEE Trans. Applied Superconductivity **25**, 1 (2015).
[9] K. Osamura, S. Machiya, Y. Tsuchiya, H. Suzuki, T. Shobu, M. Sato, S. Harjo, K. Miyashita, Y. Wadayama, S. Ochiai, and A. Nishimura, "Thermal strain exerted on superconductive filaments in practical Nb_3Sn and Nb_3Al strands," Supercond. Sci. Technol. **26**, 094001 (2013).
[10] H. Oguro, S. Awaji, K. Watanabe, M. Sugano, S. Machiya, T. Shobu, M. Sato, T. Koganezawa, and K. Osamura, "Internal strain measurement for Nb_3Sn wires using synchrotron radiation," Supercond. Sci. Technol. **25**, 054004 (2012).
[11] D. Arbelaez, A. Godeke, and S. O. Prestemon, "An improved model for the strain dependence of the superconducting properties of Nb_3Sn," Supercond. Sci. Technol. **22**, 025005 (2009).

[12]D. M. J. Taylor and D. P. Hampshire, "The scaling law for the strain dependence of the critical current density in Nb_3Sn superconducting wires," Supercond. Sci. Technol. **18**, S241–S252 (2005).
[13]D. S. Easton and R. E. Schwall, "Performance of multifilamentary Nb_3Sn under mechanical load," Apply. Phys. Letter **29**, 319 (1976).
[14]N. Cheggour, A. Nijhuis, H. J. G. Krooshoop, X. F. Lu, J. Splett, T. C. Stauffer, L. F. Goodrich, M. C. Jewell, A. Devred, and Y. Nabara, "Strain and magnetic-field characterization of a bronze-route Nb_3Sn ITER wire: Benchmarking of strain measurement facilities at NIST and University of Twente," IEEE Trans. Appl. Supercond. **22**, 4805104 (2012).
[15]K. Osamura, S. Machiya, S. Harjo, T. Nakamoto, N. Cheggour, and A. Nijhuis, "Local strain exerted on Nb_3Sn filaments in an ITER strand," Supercond. Sci. Technol. **28**, 045016 (2015).
[16]J. W. Ekin, "Strain scaling law for the flux pinning in practical superconductors. Part 1: Basic relationship and application to Nb_3Sn conductor," Cryogenics **20**, 611 (1980).
[17]K. Osamura, S. Machiya, D. P. Hampshire, Y. Tsuchiya, T. Shobu, K. Kajiwara, G. Osabe, K. Yamazaki, Y. Yamada, and J. Fujikami, "Uniaxial strain dependence of the critical current of DI-BSCCO tapes," Supercond. Sci. Technol. **27**, 085005 (2014).
[18]C. Senatore, C. Barth, M. Bonura, M. Kulich, and G. Mondonico, "Field and temperature scaling of the critical current density in commercial REBCO coated conductors," Supercond. Sci. Technol. **29**, 014002 (2016).
[19]H.-S. Shin and Z. Bautista, "Establishing a test procedure for evaluating the electromechanical properties of practical REBCO coated conductor tapes by the uniaxial tension test at 77 K," Supercond. Sci. Technol. **32**, 064004 (2019).
[20]K. Osamura, S. Machiya, and D. Hampshire, "Mechanism for the uniaxial strain dependence of the critical current in practical REBCO tapes," Supercond. Sci. Technol. **29**, 065019 (2016).
[21]P. Sunwong, J. S. Higgins, and D. P. Hampshire, "Angular, temperature and strain dependence of the critical current of DI-BSCCO tapes in high magnetic fields," IEEE Trans. Appl. Supercond. **21**, 2840–2844 (2011).
[22]http://www.superpower-inc.com/content/2g-hts-wire.
[23]http://www.fujikura.com/solutions/superconductingwire/.
[24]IEC 61788-25:2018 Superconductivity – Superconducting wires - Mechanical properties measurement – Room temperature tensile test on REBCO wires.
[25]D. M. J. Taylor and D. P. Hampshire, "Properties of helical springs used to measure the axial strain dependence of the critical current density in superconducting wire," Supercond. Sci. Technol. **18**, 356–368 (2005).
[26]J. R. Greenwood, E. Surrey, and D. P. Hampshire, "The biaxial strain dependence of J_C of a (RE)BCO coated conductor at 77 K," IEEE Trans. Appl. Super. **29**(5), 1 (2019).
[27]S. Awaji *et al.*, "Strain-controlled critical temperature in $REBa_2Cu_3O_y$-coated conductors," Sci. Rep. **5**, 11156 (2015).